Thesis for the Degree of Master of Engineering

Upconversion Luminescence Properties of Er^{3+}/Yb^{3+} codoped $KY(MoO_4)_2$ phosphor

by

Quynh Thi Vu

Interdisciplinary Program of

Biomedical, Mechanical & Electrical Engineering

The Graduate School

Pukyong National University

January, 2017

Upconversion Luminescence Properties of Er^{3+}/Yb^{3+} codoped $KY(MoO_4)_2$ phosphor

Er^{3+}및 Yb^{3+}이온이첨가된 $KY(MoO_4)_2$ 형광체의상방전환형광특성연구

Advisor: Prof. Hyo Jin Seo

by

Quynh Thi Vu

A thesis submitted in partial fulfillment of the requirements

for the degree of

Master of Engineering

in Interdisciplinary Program of Biomedical, Mechanical &

Electrical Engineering, the Graduate School,

Pukyong National University

January, 2017

Upconversion Luminescence Properties of Er^{3+}/Yb^{3+} codoped $KY(MoO_4)_2$ phosphor

A dissertation

by

Quynh Thi Vu

Approved by:

_____

(Chairman: Professor Cheol Woo Park)

_____

(Member: Ph.D. Kyoung Hyuk Jang)

_____

(Member: Professor Hyo Jin Seo)

January, 2017

Contents

List of Figures

List of Tables

Upconversion Luminescence Properties of Er^{3+}/Yb^{3+} codoped $KY(MoO_4)_2$ phosphor

Quynh Thi Vu

Interdisciplinary Program of Biomedical, Mechanical & Electrical Engineering

Pukyong National University

Abstract

$KY(MoO_4)_2$: 1%Er^{3+}/x%Yb^{3+} (x=5% ~ 99%) (KYM: Er^{3+}/Yb^{3+}) solid solutions were prepared by conventional solid state reaction method with fixed Er^{3+} at 1% mol and various Yb^{3+} concentration from 5 to 99% mol. A systematic structural of the solid solution series was carried out by X-ray powder diffraction. The typical diffraction peaks reveal a systematic shift to angle, confirming the formation of a solid solution. The luminescence characteristic is investigated by using upconversion measurement under the laser excitation at 975 nm.

Under 975 nm excitation laser, three emission band: blue, green and red emissions centered at (410 nm, 480 nm), (532 nm, 546 nm) and 673 nm, respectively, are observed for the series KYM: Er^{3+}/Yb^{3+}. It is noticeable

that the green band (transition $^2H_{11/2}$/ $^4S_{3/2}$→ $^4I_{15/2}$ of Er^{3+}) is much higher than the blue band (transition $^2H_{9/2}$/$^2H_{7/2}$ → $^4I_{15/2}$ of Er^{3+}) and red emission (transition $^2F_{9/2}$ → $^4I_{15/2}$ of Er^{3+}). Moreover, with increasing the Yb^{3+}, the intensity increases with high concentration quenching and energy transfer occurs between Yb^{3+}-Er^{3+} couples. Two and three-photon excitation processes being responsible for the various emission bands were confirmed. Finally, based on laser pump power, the energy transfer between Yb^{3+}/Er^{3+} are discussed in detail.

1. Introduction

Upconversion luminescence properties of Er^{3+}/Yb^{3+} codoped in double molybdates compounds $KY(MoO_4)_2$ are interested. Over the past several decades, upconversion (UC) luminescence in rare earth (RE) ions doped materials has been intensively studied due to their potential applications in many fields, such as three-dimensional displays, optical data storage, medical diagnostics, sensors, lasers and optical amplifiers [1-5]. Er^{3+}, Tm^{3+}, Pr^{3+}, Nd^{3+}, and Ho^{3+} are favorite trivalent RE ions being used as luminescence centers for UC materials. More interestingly, Er^{3+} is the most efficient rare earth for upconversion because Er^{3+} with rich energy levels shows the luminescence quenching at high concentration. In addition, Er^{3+} ions give some suitable intermediate levels so it is easily radiate in the near infrared region [6]. However, under the 975 nm infrared excitation, the ground state absorption (GSA) of Er^{3+} is very weak, that leads to low pump efficiency. Because of these disadvantages of Er^{3+}, Yb^{3+} is well known as a common and interesting sensitizer because Yb^{3+} has high absorption cross-section and broad absorption band around 975 nm, that is the reason why Yb^{3+} is used to enhance the upconversion efficient [7]. Moreover, double molybdates $KY(MoO_4)_2$ has many advantages to being a good efficient luminescence like showing high efficiency, hydrolytic stability, mechanical stability, excellent thermal and easy to dope a large number of the rare-earth ions. Due to their reasons, it seems interesting to investigate the luminescence properties of $KY(MoO_4)_2$ doping rare earth.

This study has contents as follows. In chapter 2, the introduction of the lanthanides ions, excitation process, energy transfer, upconversion mechanisms and upconversion materials are briefly reviewed. Chapter 3 shows the measurements using to investigate the structure and the optical characteristic with a description of an experiment setup and sample preparation. Experiments results are finally presented and discussed in Chapter 4.

2. Background and Theory

2.1. The lanthanides

Rare earth (RE) with most complicated optical spectra because they have rich energy levels of the 4f-4f transitions are used extensively in luminescent materials. The 4f electrons are well shielded from the surroundings by the outside shells of $5s^2 5p^6$, therefore, in a configurational coordinate diagram these levels were shown as parallel parabolas ($\Delta R=0$) and the transitions within the 4f configurations are forbidden for the electric dipole transitions by the parity selection rule. However, they are usually observed in some crystals due to the effect of special crystal field which mixes some different parity states into the 4f states. For the trivalent rare earth ions, the $4f^n$ configuration is relatively isolated many line emissions can be obtained due to the 4f-4f transitions [8-11].

In different host lattice, the optical properties of a luminescent center are different too because the ions experience the different surroundings such a center. This is easy to understand since we change the direct surroundings of the luminescent centers, the properties of the sample may change also. The first factor is a reason why in a different host, different spectral properties of a given ion lattice is covalency [11]. The interaction between the electrons is reduced in order to increase covalency because they spread out over wider orbitals. Because of that, electronic transfers between different energy levels with a different energy which is calculated by electron interaction difference to lower energy for increasing covalency.

This phenomenon is called nephelauxetic effect. The crystal field is another factor affecting the optical properties of an excited ion in a given host lattice. Due to the surroundings, that is the electric field at the site of the ion under consideration. By using the strength of the crystal field, the position of certain optical transitions is calculated, the most well-known and clear example is the transitions metal ions. Compare with the general RE-doped oxide-based host materials, the Rare-earth doped molybdate phosphors have high Chemical stability and have been extensively explored as efficient phosphors. What's more, molybdate phosphors can provide unshakeable properties with destruction under excitation of ultraviolet light [12-15].

Rare earth ions are important in the development of laser hosts since the electrons involved in optical phenomena are relatively insensitive to the crystal field of the surrounding host materials. The lanthanide ions are the most interesting doped ion in many host lattice. They are a group of elements found at the bottom of the periodic table. The electronic configuration of the rare-earth ions is $[Xe]4f^n5s^25p^6$ where n varies from 0 to 14 (with the exception of Gadolinium which has an extra 5d electron). Figure 2.1 represents a real part of the energy levels which originates from the $4f^n$ configuration. This figure shows as a function of n for the trivalent rare-earth ions. The typical optical transitions of rare-earth spectra are attributed to intra-4f electric-dipole transitions of electrons already in the 4f shell to these unoccupied 4f levels. The number of configurations for n electrons which is divided over the fourteen 4f orbitals is large. Due to

that, all configurations have different energy, giving increase to energy levels in the UV, visible and near infra-red part of the spectrum.

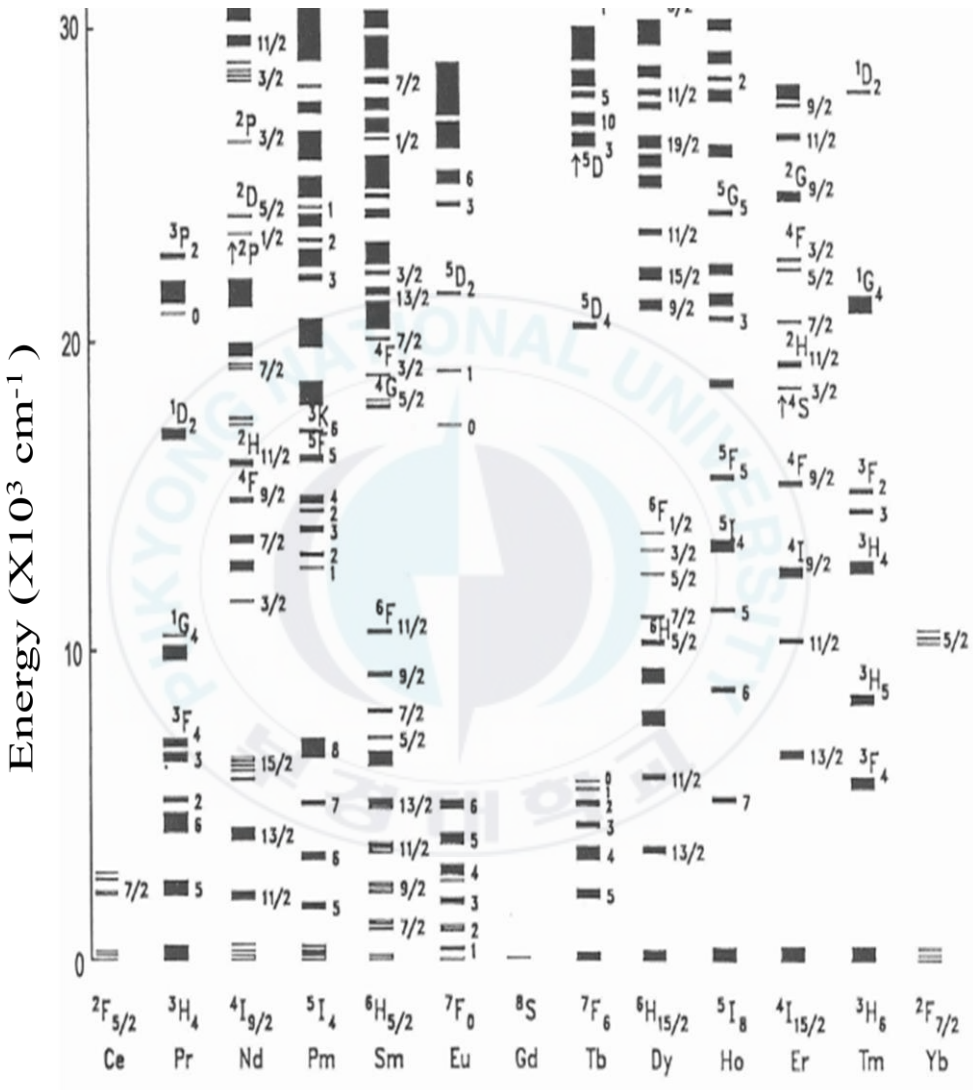

Figure 2.1. Energy levels of $4f^n$ configurations of the trivalent rare-earth below 30,000 cm^{-1} .

This diagram shows the energy level structure of the $4f^n$ configuration of trivalent lanthanide ions, which clearly shows the high energy level structure of these ions. It is also a representation of the 4f energy level structure of these ions when doped into various kinds of crystalline or glassy materials. Moreover, the 4f orbital is shielded by the filled $5s^2$ and $5p^6$ orbitals from the surroundings and lies inside the ion and. Consequently, the host lattice influent on the optical transitions within the $4f^n$ configuration essentially but it is a small effect. From Figure 2.1, the order of magnitude of the crystal field splitting is given by the width of the bars. It is seen to be very smaller than the transition metal ions.

2.2. Lanthanide excitation process

2.2.1. 4f-4f transition

4f-4f transitions are important in spectroscopy and will be focused in this thesis.

4f-4f transition includes the migration of electrons between different energy levels of the 4f orbitals in the same lanthanide ion. 4f-4f electric-dipole transitions are in theory forbidden by the parity rule. Although they are in practice generally observed, the corresponding emission bands are usually not strong and narrow.

2.2.2. 4f-5d transition

In 4f-5d transitions, one of the electrons locating at 4f orbital is excited

to a 5d orbital of higher energy. This excitation absorption process is usually denoted $4f^n \rightarrow 4f^{n-1}5d$ and is typically observed in Ce^{3+} ions ($4f^1$ configuration). Due to that the half-filled, empty or completely filled electron shell configurations are the most remaining unchanged once, the 4f electron of Ce^{3+} is easily excited to the 5d orbital. Unlike 4f-4f transitions, the 4f-5d transitions are permitted, which emits strong and broad absorption cross-sections.

2.2.3. Charge-transfer state transition

In charge-transfer transitions, two neighboring anions - 2p electrons were (e.g. O^{2-} in oxides) transferred to a 4f orbital. It is typically observed in Eu^{3+} ($4f^6$) which need to be filled full half-filled configuration. The trivalent ions have a tendency become divalent (Sm^{3+}, Eu^{3+}, Yb^{3+}). That shows charge-transfer absorption bands in the UV band. In the less negative electron sulfides also ions like Nd^{3+}, Dy^{3+}, Ho^{3+} and Tm^{3+} show charge-transfer transitions. The transitions are permitted and give broad and intense absorption

2.3. Energy transfers process

Over several decays, there are many studies researching about the transfer of electronic transitions between dopants in solids. In this section, we focused on energy transfer processes between a donor and an acceptor or we can consider a donor like a sensitizer and an acceptor like an activator. The theory behind nonradiative sensitizers to activators energy transfer was

developed by Forster [16] and subsequently extended by Dexter [17] and Inokuti [18]. In 1952, Botden [19] introduced the notion of relaxation by migration to account for luminescence concentration quenching. His theory was further developed by Detex and Schulman [20]. The combined effects of sensitizer- sensitizer and sensitize-activator transfers have been studied extensively in a variety of rare earth doped inorganic materials systems.

Figure 2.2 shows the energy transfer process in materials doping rare earth. Firstly, a sensitizer S is excited by excitation source and jumps to higher energy level S^* then it transfers energy to an activator which is still in the ground state. After getting energy from the sensitizer, the activator is excited to higher energy level A_1^*, it may be followed by a nonradiative emission to the lower energy level A_2^* or directly emits a radiative emission. At level A_2^*, the excited activator falls down to the ground state by emitting a radiative emission.

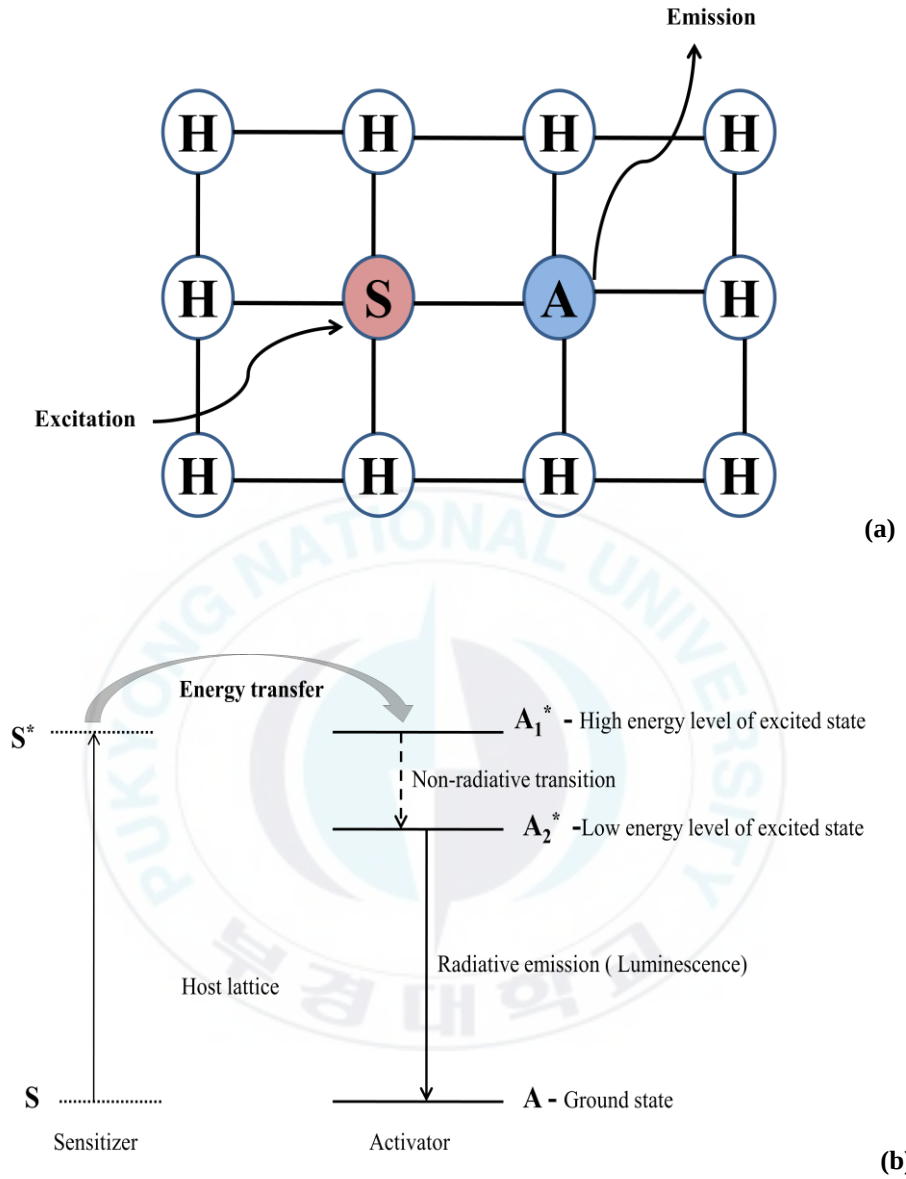

Figure 2.2 Energy transfer process in materials doping rare earth.

2.4. Upconversion mechanism

2.4.1. Upconversion mechanism

Photon upconversion is a process which generates higher-energy emission from lower-energy radiation. The enhance energy is given by absorbing multiple (usually two or three) photons for single emitted photon. The transition from the excited electronic state back to another lower-lying energy level or fall down to the ground state produces luminescence band centered at a shorter wavelength than the original excitation wavelength. This nonlinear optical phenomenon is called anti-Stokes photoluminescence, includes intermediate excited states [21].

Several upconversion mechanisms have shown in Figure 2.2, they may appear in combinations processes or alone. The most efficient mechanism is usually dominant in low excitation power density. However, when pumping power increases, it is the enabled emergence of less efficient mechanism [22]. Some upconversion processes are relatively insensitive to ion concentration and involve only one type of ion, while the others stipulate the contribution of energy transfer donor (sensitizer) and acceptor (activator) ions separating [23]. In the latter case, the upconversion mechanism is affected by the concentration and distribution of the operational ions due to the influence of the ionic distance on the energy transfer rate constant [24].

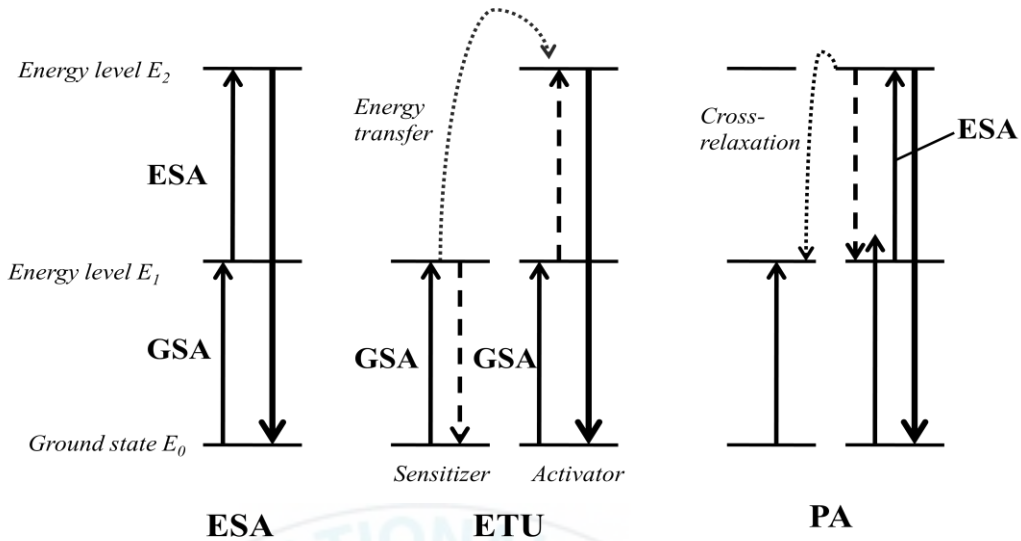

Figure 2.3 Simple energy diagrams of the most significant upconversion mechanisms. ESA: excited state absorption, GSA: ground state absorption; ETU: energy transfer up-conversion; PA: photon avalanche [25].

ESA

ESA, excited state absorption in upconversion mechanism involves only a single ion. It is the mechanism resulting in the near-infrared-to-visible photons upconversion. The first pump populates the intermediate excited state E1 (or by ground state absorption, GSA), before the second type of absorption (ESA) exciting the upconversion emissions from the higher E2 level.

ETU

ETU, Energy transfer upconversion is about a hundred times of efficient than the excited state absorption mechanism. In this case, the GSA is given a nonradiative resonant energy which transfers from the sensitizer

ions to the activator ions, then results in the population of higher excited state E2 of the latter.

PA

Photon avalanche (PA), involves cross relaxation energy transfer between neighboring ions. When the pump flux dominates a certain critical threshold, PA is a more complex mechanism observed. Because the excitation energy is not resonant with the GSA transition directly, just only with the following ESA transition, the cross relaxation process assists in a population of the intermediate excited E1. The first GSA process is strongly inefficient, but after the ESA process populates the higher excited state E2 extremely effectively. The cross relaxation process results in a population of the middle state E1 of neighboring ions, and the avalanche process is raised up. Although PA is finally a highly efficient upconversion mechanism, it is still poorly exploitable because of the slow responses to the excitation laser pump.

Cooperative luminescence and cooperative sensitization.

The cooperative luminescence process occurs among the same type of ions that are in the excited state. Two ions in the excited state combine their energy to a quantum which is emitted (however, there is no real emitting level) (Figure 2.3).

Upconversion by cooperative sensitization occurs with two different ions. Ion A transfers simultaneously its excited energy to ion C, which has no energy level at the position of the excited level of ion A. Emission

occurs from the excited state of ion C.

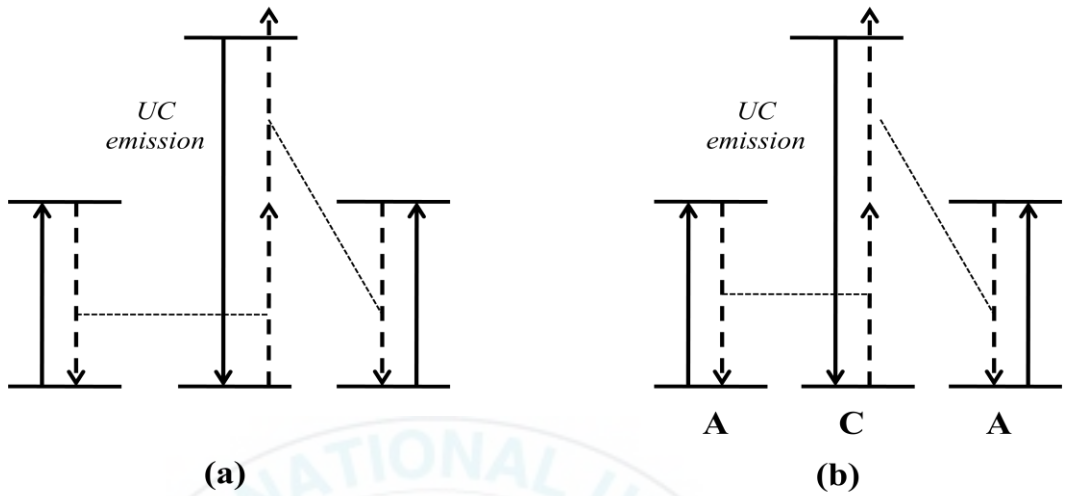

Figure 2.4 Schematic representation of the upconversion mechanism by cooperative luminescence (a) and cooperative sensitization (b).

2.4.2. Upconversion materials doping Yb^{3+} and Er^{3+}

The first sample of upconversion was reported by Auzel in 1966, it was the couple Yb^{3+}, Er^{3+} in CaW04 [26]. Like mentioned above, Yb^{3+} ion can sensitize the all of these lanthanide ions, efficiently because Yb^{3+}'s absorption is located around 975 nm and much stronger for the $^2F_{7/2} \rightarrow {}^2F_{5/2}$ transition. The Er^{3+} ions usually have three upconversion emission band, including two green emission bands centered at 525/545 nm corresponded to the transition $^2H_{11/2}/\ ^4S_{3/2} \rightarrow {}^4I_{15/2}$. Figure 2.4 shows the energy level diagram observed. Near infrared radiation (NIR-970 nm) is absorbed by Yb^{3+} and transferred to Er^{3+} leads to the $^4I_{11/2}$ level of Er^{3+} is populated. Following that, a second photon located at the $^4I_{11/2}$ level is absorbed by

Yb^{3+} and transferred that energy to Er^{3+}. The Er^{3+} ion jumped from the $^4I_{11/2}$ to the $^4F_{7/2}$ level. Next, it falls down rapidly and nonradiatively to the $^4I_{11/2}$ level from which a green emission occurs ($^4S_{3/2} \rightarrow {}^4I_{15/2}$).

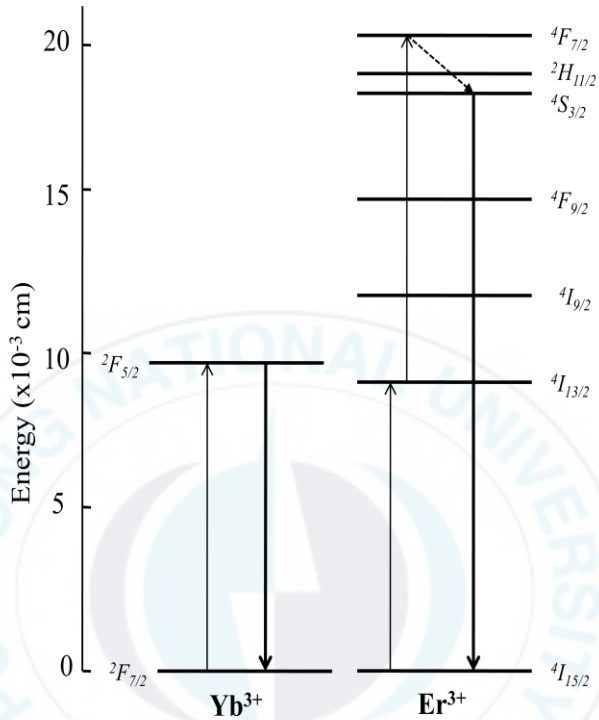

Figure 2.5 Upconversion in the Yb^{3+}, Er^{3+} couple. Excitation is into Yb^{3+}, emission from the $^4S_{3/2}$ level of Er^{3+}

Because two infrared photons are required to produce a green emission, the emission intensity will quadratically increase when the density of the excitation. This has been observed and is proof of the two-photon character of the excitation. In some case, the upconversion process requires more than two-photon taking part in the excitation process.

The number of required photons is also well known as the relative

coefficient of the luminescence emission intensity and the pump power of the laser. From the 1960s when research began this area, it was known that the up-conversion luminescence intensity is related to the nth power of the absorbed pump power P ($\boldsymbol{I \sim P^n}$), when n donates the number of pump photons required for each upconversion photon emit. In another hand, when P versus I is represented in a double logarithmic, the slope of the trend line is n. Like more powerful near infrared excitation sources become available, the saturation phenomenon of the upconversion which included luminescence was observed, and it was realized that the power dependence of the upconversion emission bands changed with excitation power [27, 28]. In the reference no 28, the authors indicated that the dependence decreases from P^n down to P^1 excitation power and, accordingly, the above-mentioned slope will approach 1 (the smallest number of photons involved). However, it is crucial to note that the excitation power has a higher impact on the luminescence intensity in the case of photon upconversion (n>1) than in the case of the common photon downconversion (n=1). There have been many researchers about the dependence of the luminescence emission intensity I on the pump power P mentioned in detail. In this works, we consider more about the dependence of the luminescence emission intensity on the concentration of the sensitizers Yb^{3+}.

3. Sample preparation and experimental measurements

3.1. Experimental chemical reagents

All the chemical reagents that were used in this experiment are shown in the table below

Table 3.1 Chemical reagents used in this experiment

Number	Name of chemical reagents	Purity	F.W.
1	K_2CO_3 (Sodium carbonate)	99.9%	138.21
2	Yb_2O_3 (Ytterbium oxide)	99.%	394.08
3	Y_2O_3 (Yttrium(III) oxide)	99.9%	225.82
4	Er_2O_3 (Erbium(III) oxide)	99.99%	382.52
5	MoO_3 (molypdenum oxide)	99.9%	143.94

3.2. Solid state reaction method

Phosphor particles are traditionally prepared by solid state reaction method with high reaction temperature for a long time period followed by

repeated ball milling process. A solid state reaction is a chemical reaction in which solvents are not used. In a normal reaction, the reacting agents also called the reactants are placed in a solvent before the reaction can take place. The reactants react to form a new substance. After the reaction is completed, researchers are able to remove the new products from the solvent. A solid state reaction, however, allows the reactants to chemically react without the presence of a solvent.

The advantages of this method ripple throughout of many industries. It is a cheaper method to buy the incident materials and prepare the sample. Producing materials from the solid state reaction will mean that the researchers are able to bypass the purification process. Eliminating the solvent from the reaction means that the solid state reaction can provide more product than any method. It also is more environmentally friendly. Since there is no solvent, there is no waste to eliminate at the end of the reaction. There are several conditions under which a solid state reaction can take place. Oven technique uses high temperature to encourage reaction without solvents. In a melting technique, the reactants are melted together. The melted reactants interact in a liquid state and become a paste which then hardens into a solid. Some reactants are highly reactive in a presence of a gas. Therefore, researchers expose substance to the stream of a reactive gas. This process is called a gas reaction.

Although there are many benefits to preparing sample by using solid state reaction, we can’t ignore its disadvantages. This method should result in a homogeneous, or uniform, substance, and some solid state reactions do

not happen. It is difficult to control the shape, size, and morphologies of the sample. Another drawback of the solid state reaction method is the introduction of the impurities in phosphor during the milling process or washing with chemicals.

3.3. Sample preparation

The $KY(MoO_4)_2$: 1%Er^{3+}/ x%Yb^{3+} ($5 \leq x \leq 99$) were syntheses by solid state reaction method in air atmosphere. According to the nominal composition $KY(MoO_4)_2$: 1%Er^{3+}/ x%Yb^{3+} ($5 \leq x \leq 99$), above starting materials were weighted by appropriate stoichiometric ratio and thoroughly mixed in an agate mortar, transferred to a crucible. The mixture powder was first pre-fired at 300°C for 5 hours in air atmosphere followed by the second heat at 650 °C for more 5 hours. The obtained powders were mixed again and heated at 800 °C for 10 h followed by a cooling process to room temperature naturally for preparation final products of solid solutions. During every step of heat treatment, the grinding and homogeneous mixing are necessary. The sample preparation process is shown in Figure 3.1.

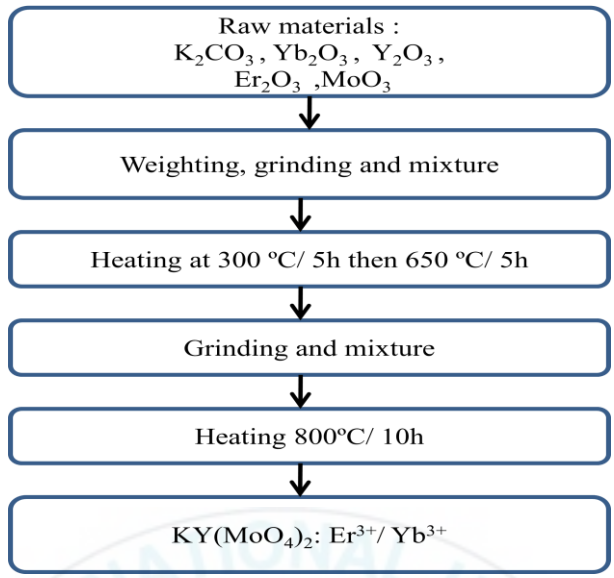

Figure 3.1 The sample preparation process

Table 3.1 The list of detailed information of the $KY(MoO_4)_2$: Yb^{3+}/Er^{3+}

No	Doping concentration		Synthesis method
	Yb^{3+}(%)	Er^{3+} (%)	
1	5	1	Solid state
2	10	1	Solid state
3	30	1	Solid state
4	50	1	Solid state
5	70	1	Solid state
6	99	1	Solid state

3.4. X-ray diffraction phase analysis

X-ray Diffraction (XRD) technique is a powerful tool for material characterization as well as for detail structural elucidation. As the physical properties of solids (e.g., electrical, optical, magnetic, ferroelectric, etc.) depend on atomic arrangements of materials, determination of the crystal structure is an indispensable part of the characterization of the materials, mainly the identification of the chemical species. An X-ray tube generates X-rays by focusing an electron beam that has been accelerated across a high voltage field and bombards a stationary or rotating solid target. As electrons collide with atoms in the target and slow down, a continuous spectrum of X-rays are emitted, which are termed Bremsstrahlung radiation. The high energy electron also ejects inner shell electrons in atoms through the ionization process. When a free electron fills the shell, the X-ray photon with an energy characteristic of the target materials is emitted. Common targets used in X-rays tubes include Cu and Mo, which emits 8keV and 14keV X-rays with corresponding wavelengths of 1.54 Å and 0.8 Å, respectively. X-ray primarily interact with electrons in atoms. Diffracted waves from different atoms can interfere with each other and the resultant intensity distribution is strongly modulated by this interaction. Of the atoms are arranged in a periodic fashion, as in crystals, the diffracted waves consist of sharp interference maxima (peak) with the same symmetry as in the distribution of atoms. Measuring the diffraction pattern, therefore, allows us to deduce the distance between crystal planes. X-ray Diffraction patterns are used to establish the atomic arrangement of

the structure of the materials because of d spacing of diffraction planes is one of the orders of X-ray wavelength λ, the various orders n of the reflection occur only at the precise values of angle θ, which satisfies the Bragg equation given by nλ=2dsinθ. The peak intensities are determined by the types and positions of the atoms in crystal lattice according to the structure factor F(hkl) : x_n

$$F(hkl)= \sum_{n=1}^{N} f_n exp[2\pi i(hx_n + ky_n + lz_n)] \quad (3.1)$$

where hkl are the Miller indices of the reflecting planes, f_n is the atomic scattering factors, and x_n, y_n, z_n are the coordinates of the n^{th} atom in the unit cell containing N atoms.

Reflection geometry as shown in Figure 3.2 was used for our measurements.

The following information can be obtained from their X-ray powder diffraction graph:

- Quality and confirmation of the prepared samples
- The interplanar spacing of the reflections
- The unit cell dimensions and lattice type

In this case, The X-ray powder diffraction (XRD) analysis was done on a Rigaku D/Max diffractometer operating at 36 kV and 25 mA using Cu Kα radiation (λ=1.5405Å)

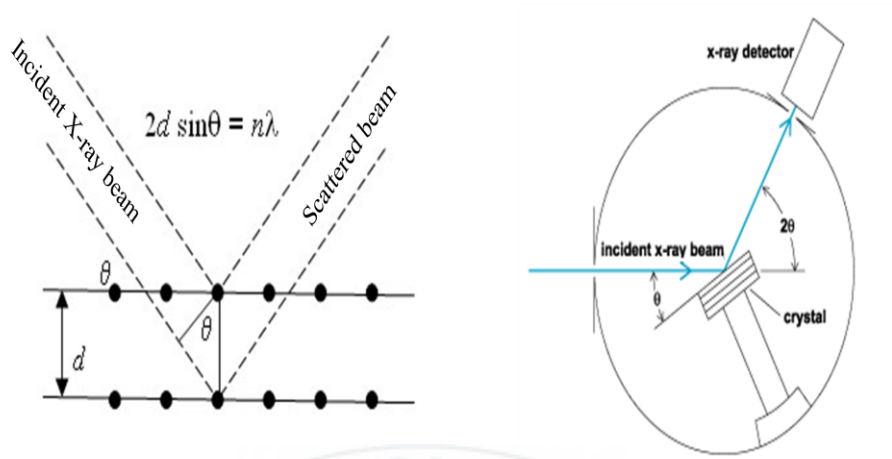

Figure 3.2. Bragg equation imitation and the X-ray diffraction experimental setup

3.5. Upconversion photoluminescence measurement under 975 nm laser diode

The experimental setup used for the upconversion emission spectra acquisition is shown in Figure 3.3. Before taking a measurement, the sample was finely ground and covered by plates. The sample holder was placed in front of the 975 nm laser diode. For the acquisition of upconversion luminescence spectra under near infrared excitation, the sample of interest was excited by using the 975 nm output of a temperature controlled cw laser diode (Thorlabs, ITC4005). The excitation signal was focused onto the center of the sample by using focus lens. Suitable filters were used to eliminate the intense laser scattering.

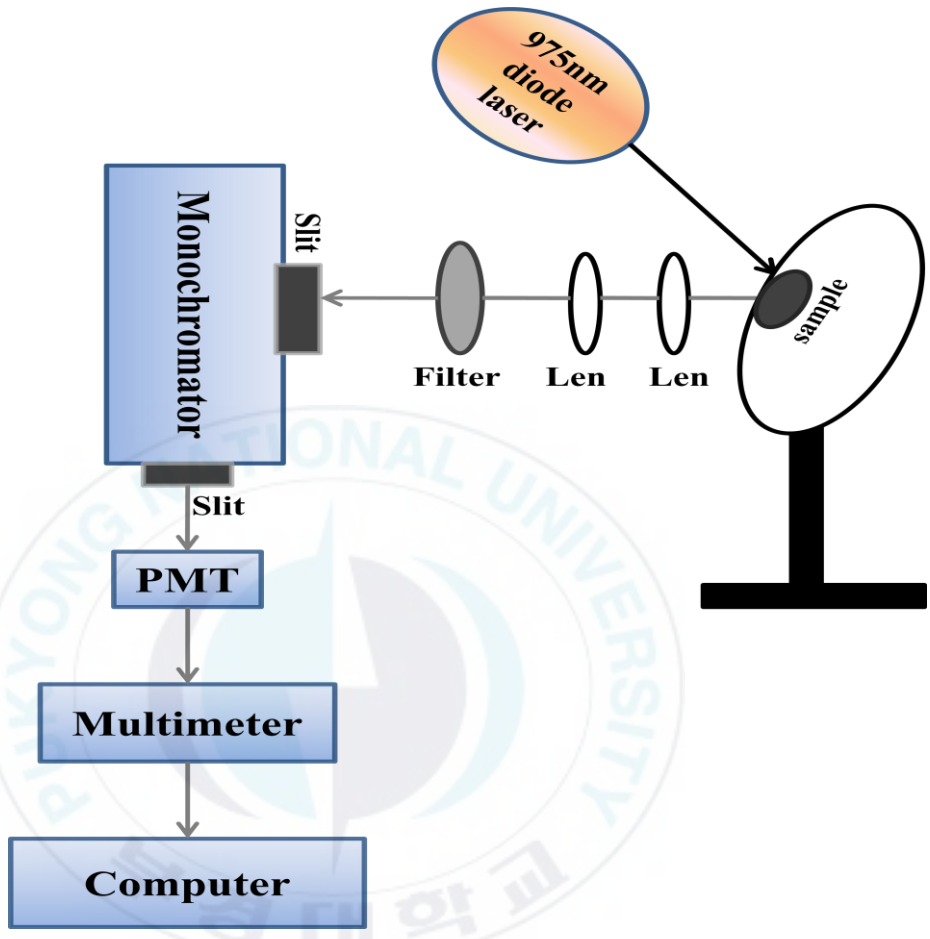

Figure 3.3 Schematic of the setup of the experiment used for upconversion measurement.

4. Result and discussion

4.1. Structure and phase formation

4.1.1. Structure description

Figure 4.1 is the corresponding schematic views of $KY(MoO_4)_2$. It can be seen that all the crystals of the double molybdate family have a layer structure and split easily into thin plates. Typically b-axis is perpendicular to splitting plane. The layered potassium - yttrium double molybdate has an orthorhombic of the crystal structure space group Pbcn (60) and contains four formulae units per elementary cell. The cell parameters are a= 5.0700 Å, b=18.2300 Å, c=7.9500 Å, and V=734.79 $Å^3$. The Y^{3+} ion is surrounded by eight oxygens while the Mo^{4-} ion is surrounded by 4 oxygens.

Table 4.1 shows the detailed information about atomic parameters of $KY(MoO_4)_2$ lattice. From Figure 4.1 and Table 4.1, it is easy to realize that a pair of Y^{3+}-Y^{3+} and Y^{3+}-K^- is connected by sharing two O^{2-} ions.

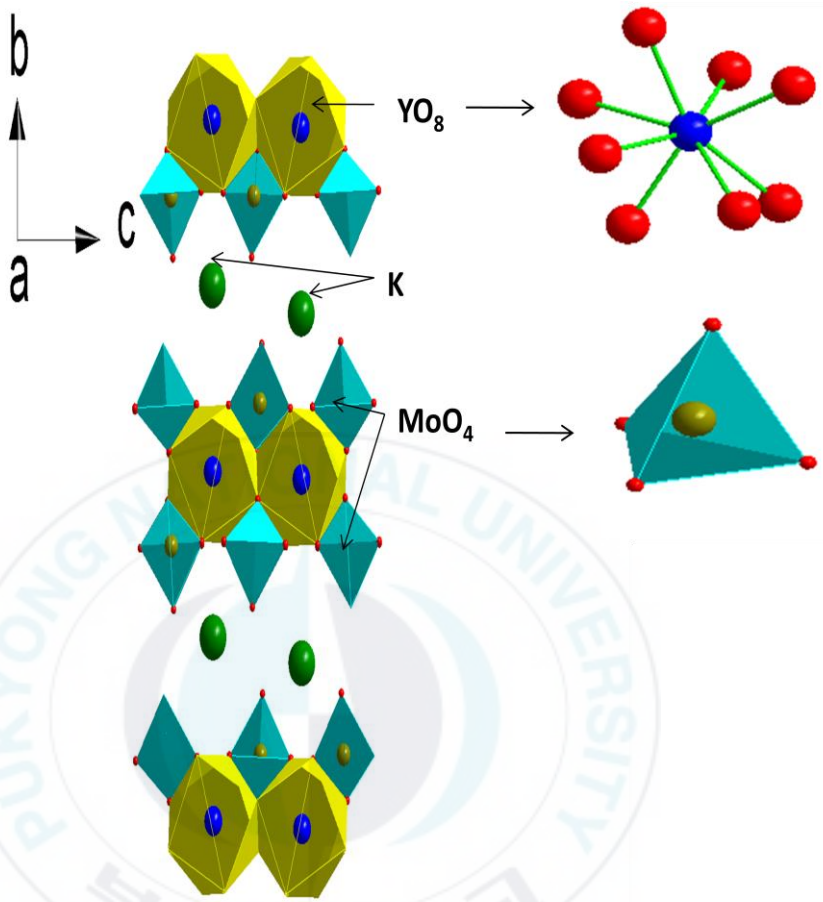

Figure 4.1. Schematic crystal structure of $KY(MoO_4)_2$

Table 4.1. Atomic parameters of $KY(MoO_4)_2$

Atom	Ox.	Wyck.	Site	x/a	y/b	z/c
Mo1	6	8d	1	0.5229(5)	0.1013(1)	-0.0161(3)
Y1	3	4c	2	0	0.0061(2)	1/4
K1	1	4c	2	1/2	0.2696(5)	1/4
O1	-2	8d	1	0.726(5)	0.100(1)	0.159(3)
O2	-2	8d	1	0.747(5)	0.095(1)	-0.187(3)
O3	-2	8d	1	0.252(4)	0.035(1)	0.004(3)
O4	-2	8d	1	0.398(5)	0.189(1)	-0.028(4)

4.1.2. Phase formation

$KY(MoO_4)_2$: 1%Er^{3+}/ x%Yb^{3+} ($5 \leq x \leq 99$) products crystallized as orthorhombic are in accordance with the reference from ICSD database no. 20478 for the samples doped with Yb^{3+} ions (0 ~ 50%). For the sample

doped with 70 and 99% of Yb^{3+} ions, the XRD peaks changed pointing to some structure alternations, which totally agree with the database card no JCPDS 52-1688 of $KYb(MoO_4)_2$. This point is easy to understand because, when the doped Yb^{3+} content increases, the XRD patterns change gradually from the $KY(MoO_4)_2$ phase to the $KYb(MoO_4)_2$ phase. Moreover, the difference between the ionic radius of Yb^{3+}, Er^{3+}, Y^{3+} is small with 0.98 Å,1.01 Å, 1.02 Å, respectively [29] so that both of the structure of KYM are the space group Pbcn (60) - orthorhombic.

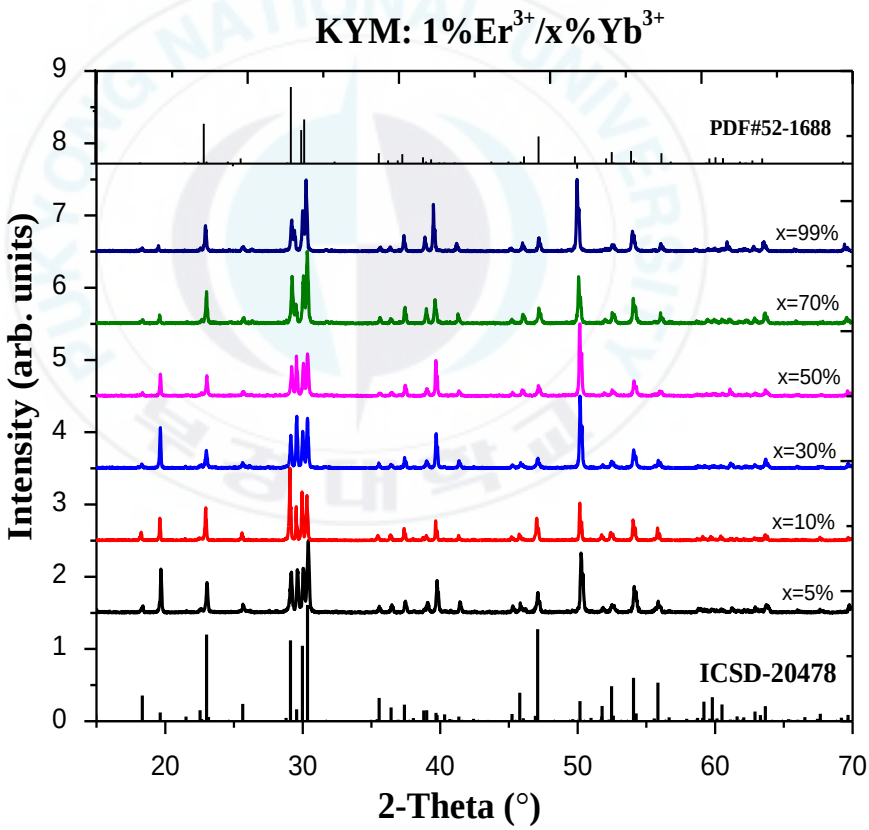

Figure 4.2 XRD patterns of KYM: 1% Er^{3+}/x%Yb^{3+} and doping with various concentration of Yb^{3+}.

4.2. Upconversion luminescence

Figure 4.3 shows the upconversion luminescence spectra of the samples KYM: 1%Er^{3+}/x%Yb^{3+} (x=5, 10, 30, 50, 70%) under 975 nm excitation. In Figure 4.3, the emission of Er^{3+} is clearly observed for all the samples with various Yb^{3+} concentrations from 5 to 70 % and it becomes stronger at high Yb^{3+} concentration. Two emission bands centered at 532, 546 (green) and 673 nm (red), which are assigned to the transitions of $^2H_{11/2} \rightarrow {}^4I_{15/2}$, $^4S_{3/2} \rightarrow {}^4I_{15/2}$, and $^2F_{9/2} \rightarrow {}^4I_{15/2}$ of Er^{3+}, respectively, are clearly observed. It is noted that the green band is much higher than the red band. Figure 4.4 shows the partial upconversion spectrum of the sample KYM: 1% Er^{3+}/50% Yb^{3+}. In Figure 4.4, the emission centered at 410 nm and 480nm corresponding to the transitions $^2H_{9/2} \rightarrow {}^4I_{15/2}$ and $^2H_{7/2} \rightarrow {}^4I_{15/2}$, respectively, are presented and their emission intensity are weak. Table 4.2 shows the relative emission intensity of KYM: 1%Er^{3+}/50%Yb^{3+} samples at the different band. The emission intensity of band centered at 410 and 480 nm are about 400 times smaller than the green band at 532nm.

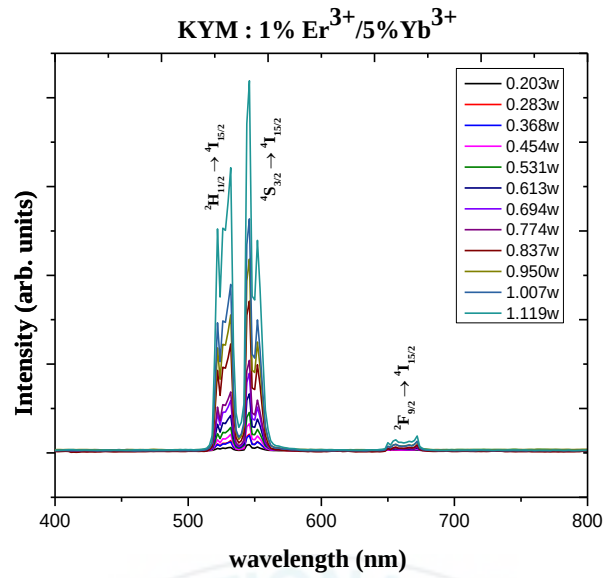
KYM : 1% Er3+/5%Yb3+
Intensity (arb. units)
wavelength (nm)
400
500
600
700
800
0.203w
0.283w
0.368w
0.454w
0.531w
0.613w
0.694w
0.774w
0.837w
0.950w
1.007w
1.119w
2H11/2 → 4I15/2
4S3/2 → 4I15/2
2F9/2 → 4I15/2

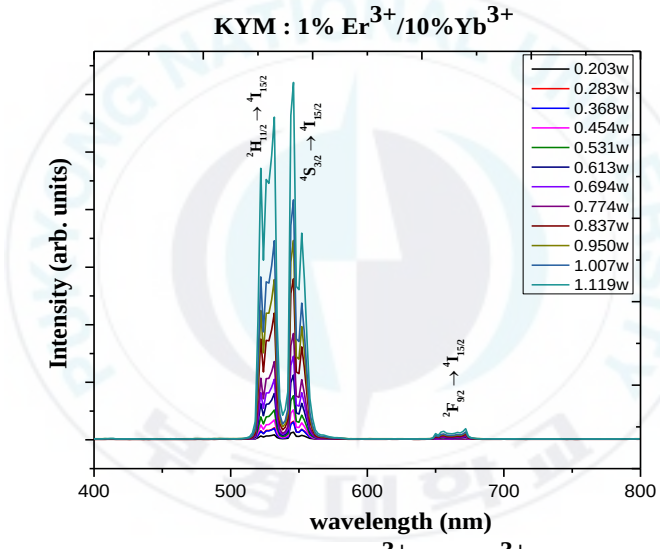
KYM : 1% Er3+/10%Yb3+
Intensity (arb. units)
wavelength (nm)
400
500
600
700
800
0.203w
0.283w
0.368w
0.454w
0.531w
0.613w
0.694w
0.774w
0.837w
0.950w
1.007w
1.119w
2H11/2 → 4I15/2
4S3/2 → 4I15/2
2F9/2 → 4I15/2

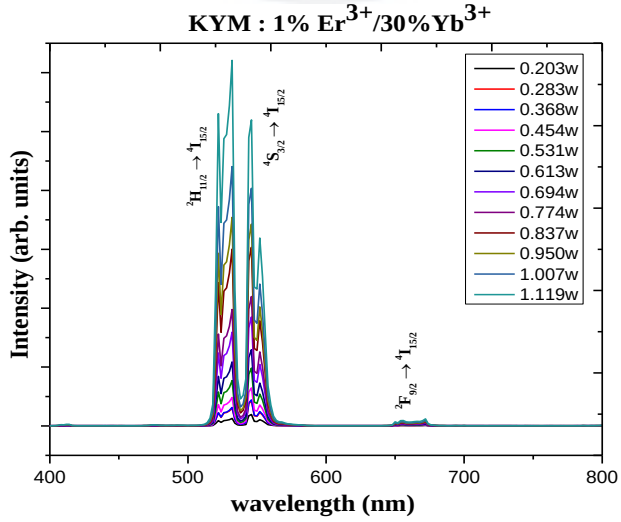
KYM : 1% Er3+/30%Yb3+
Intensity (arb. units)
wavelength (nm)
400
500
600
700
800
0.203w
0.283w
0.368w
0.454w
0.531w
0.613w
0.694w
0.774w
0.837w
0.950w
1.007w
1.119w
2H11/2 → 4I15/2
4S3/2 → 4I15/2
2F9/2 → 4I15/2

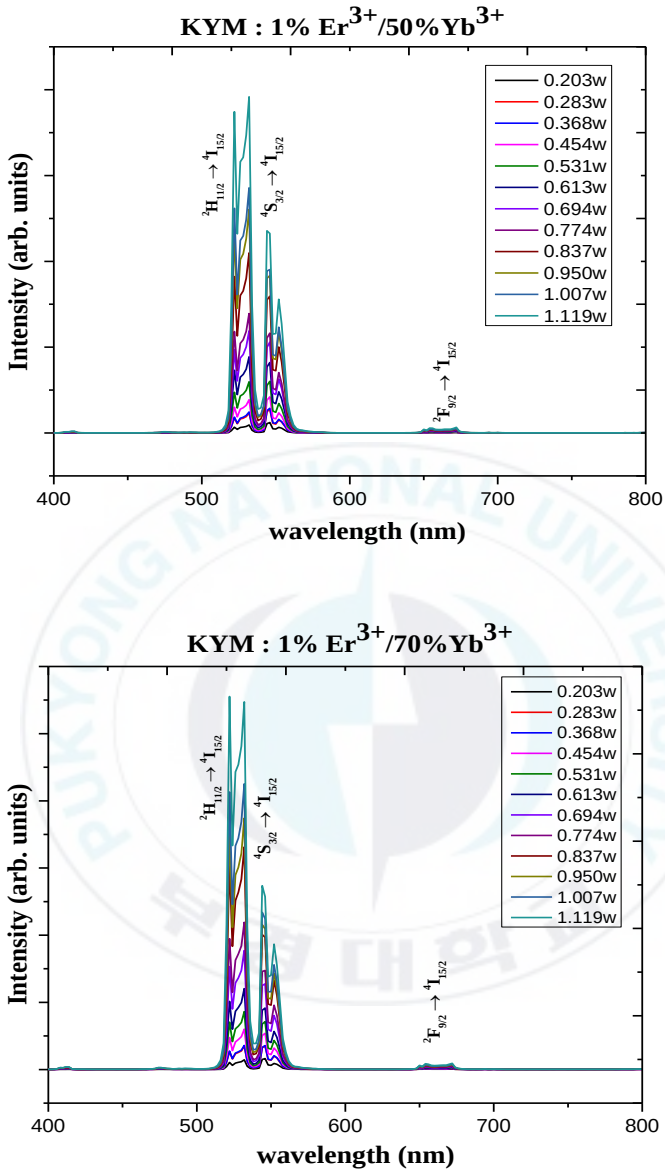

Figure 4.3 Upconversion emission spectrum of the samples excited by 975 nm LD: KYM: 1% Er^{3+}/x% Yb^{3+} (x=5, 10, 30, 50, 70 %).

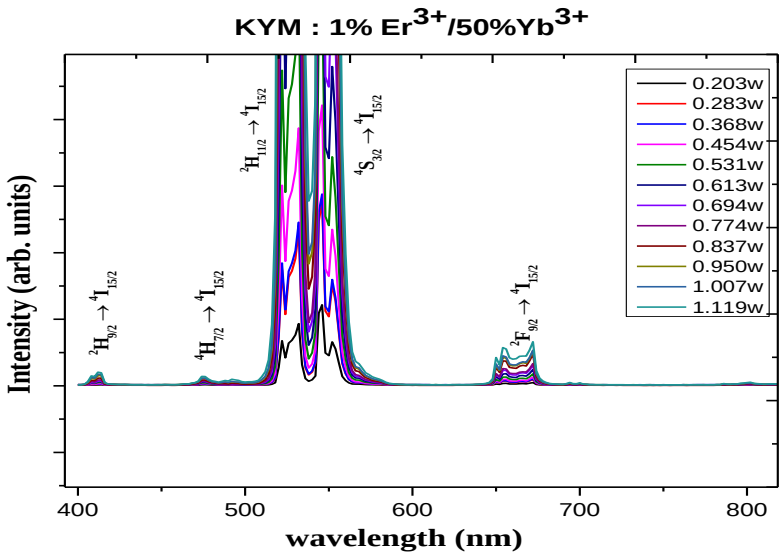

Figure 4.4 The partial upconversion spectrum of the sample KYM: 1% Er^{3+}/50% Yb^{3+} when take the room out in detailed.

Table 4.2 The relationship of the emission intensity of KYM: 1%Er^{3+}/50%Yb^{3+} samples at the different band.

Band Centered	Transition of Er^{3+}	Emission intensity at power 1.119W excitation of KYM: 1%Er^{3+}/50%Yb^{3+}
410 nm	$^2H_{9/2} \rightarrow {}^4I_{15/2}$	0.00279
480 nm	$^2H_{7/2} \rightarrow {}^4I_{15/2}$	0.00154
532 nm	$^2H_{11/2} \rightarrow {}^4I_{15/2}$	0.78326
546 nm	$^4S_{3/2} \rightarrow {}^4I_{15/2}$	0.47125
673 nm	$^2F_{9/2} \rightarrow {}^4I_{15/2}$	0.01322

Dependence of upconversion emission on sensitizer Yb^{3+} concentration

One of the factors affecting the luminescent performance is the doping concentration of the rare-earth in the host lattice. When s rare-earth ion doped in host lattice, it will replace a host cation. When Yb^{3+} and Er^{3+} are doped in $KY(MoO_4)_2$ lattice in a prepared suitable stoichiometric, they replace the Y^{3+} ions in $KY(MoO_4)_2$ lattice. As mentioned above, the Yb^{3+} ion acts a sensitizer and the Er^{3+} ion acts as an activator, so the concentration of Yb^{3+} and Er^{3+} totally affects to the luminescent intensity. In the thesis, the dependence of upconversion luminescence on Yb^{3+} concentration of $KY(MoO_4)_2$: $1\%Er^{3+}/x\%Yb^{3+}$ phosphors is investigated. Figure 4.5(a) shows the upconversion emission spectrum of the series the sample $KY(MoO_4)_2$: $1\%Er^{3+}/x\%Yb^{3+}$ (x = 0 ~70%) under 975 nm excitation.

From Figure 4.5(a), the emission band of Er^{3+} is obtained which are centered at 532 nm ($^2H_{11/2} \rightarrow {}^4I_{15/2}$), 546 nm ($^4S_{3/2} \rightarrow {}^4I_{15/2}$) and 673 nm ($^2F_{9/2} \rightarrow {}^4I_{15/2}$). Meanwhile, the blue emission centered at 410 nm ($^2H_{9/2} \rightarrow {}^4I_{15/2}$) and 480 nm ($^2H_{7/2} \rightarrow {}^4I_{15/2}$) are weak.

The dependence of upconversion luminescence intensity on Yb^{3+} concentration was presented in Figure 4.5(b) for the green and red band. It is indicated that firstly, the emission intensity increase and reach the maximum at 50% of Yb^{3+} concentration for both green and red band. The intensity begins falling down when the Yb^{3+} concentration continuously

increases. It is concluded that 50% Yb^{3+} concentration doping in the host lattice is optimum concentration to dope in the phosphor.

To explain the quenching phenomenon, a quenching mechanism was depicted in details. Fig 4.8 shows the energy level diagram illustrating the proposed energy migration mechanisms of Er^{3+}/Yb^{3+}. When the phosphor samples were excited by 975 nm laser diode, the Er^{3+} was populated at excited energy level through getting energy from energy transfer (ET from Yb^{3+}) or excited state absorption (ESA) process. The excited state energy level is mainly populated by ESA (Er^{3+} was directly excited by laser beam and transit to the higher state) when Yb^{3+} concentration is lower. However, when Yb^{3+} concentration is higher, the ET processes is dominant which leads the population of Er^{3+} at excited state energy level is more crowded. As mentioned in chapter 2, high dopant concentrations favor high energy transfer rates between sensitizers and activators. In some case, the excitation energy can relocate far away from the activator which had initially absorbed the incident photon, and eventually get trapped by non-luminescent defect or impurity. This process leads to a reduction of luminescence efficiency.

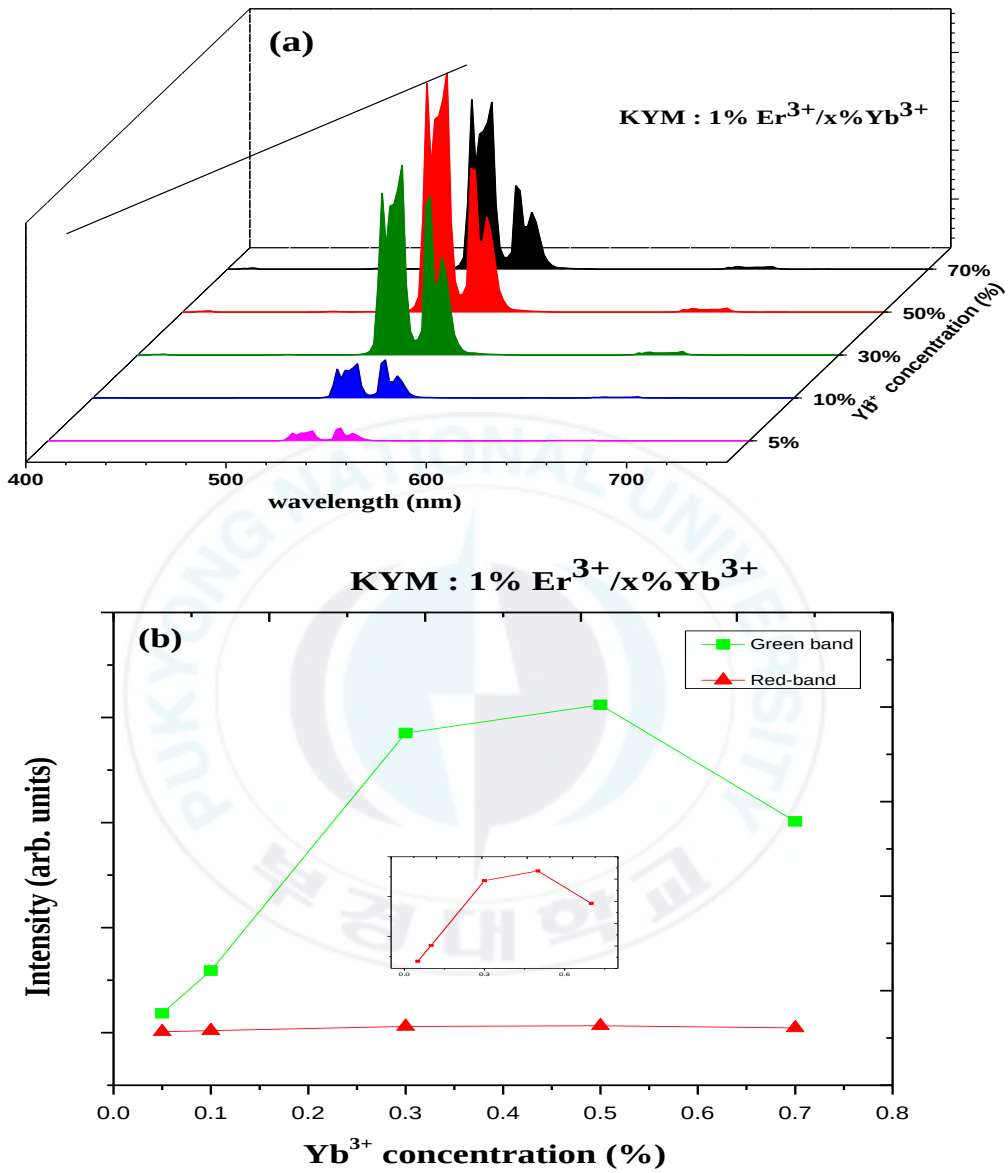

Figure 4.5 (a) The upconversion spectrum of KYM: 1%Er^{3+}/x%Yb^{3+} (x=5~70%) excited by 975 nm LD, (b) the dependence of upconversion luminescence intensity on Yb^{3+} concentration.

Power dependence of upconversion emission spectrum

The second factor affecting the upconversion luminescent performance is the power of the excitation laser. Figure 4.6 shows the upconversion spectrum of the sample KYM: 1%Er^{3+}/50%Yb^{3+} excited by 975 nm laser diode under different laser power. In Figure 4.6, the green band emission (centered at 532 and 546 nm) corresponding to the transition $^2H_{11/2}$/ $^4S_{3/2}$ → $^4I_{15/2}$ was clearly obtained. It is noticed that the intensity of the emission increases when the laser pump power increases. In detail, for the peak at 532 nm, the emission intensity excited by 1.119 W laser power is four times higher than that one excited by 0.613W laser power, while it is three times higher for the peak centered at 546 nm. Table 4.3 shows the list of the intensity of the emission band excited by different laser power.

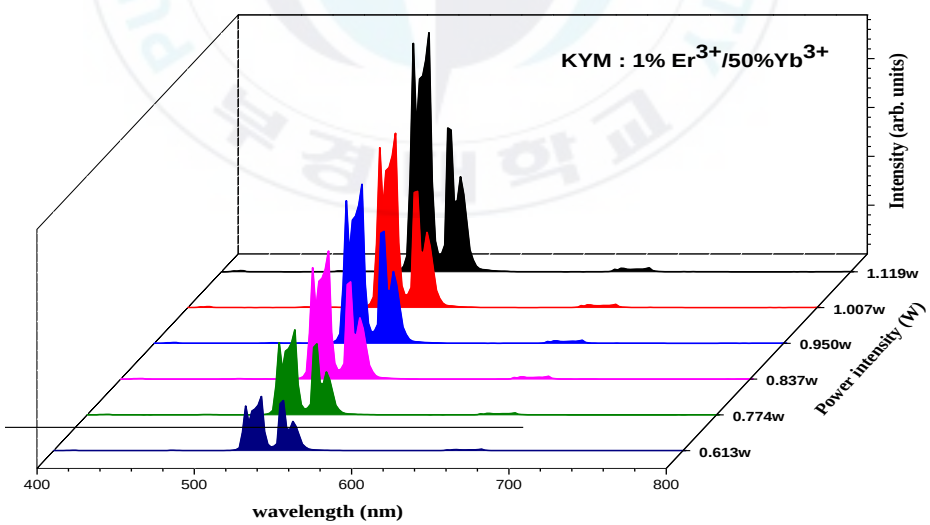

Figure 4.6 Upconversion spectrum of the sample KYM: 1%Er^{3+}/50%Yb^{3+} excited by 975 nm LD under different laser power.

Table 4.3 The list of the intensity of the emission band excited by different pump power.

Pump power (W)	Intensity of peak 532 nm ($^2H_{11/2} \rightarrow {}^4I_{15/2}$) (a.u)	Intensity of peak 546 nm ($^4S_{3/2} \rightarrow {}^4I_{15/2}$) (a.u)
0.613	0.17747	0.1644
0.774	0.2784	0.23263
0.837	0.41968	0.31877
0.950	0.52114	0.36691
1.007	0.57125	0.38103
1.119	0.78326	0.46487

As mentioned in chapter 2, in solid state materials doping rare-earth, the main excitation process is energy transfer upconversion (ETU). For an upconversion process, the luminescence intensity (I_{UC}) is proportional to the laser pump power density (P) according to the following equation:

$$I_{UC} \sim P^n \quad \text{with n is an integer parameter}$$

Where n is the number of pump photons being required to take part in the absorption? P is laser pump power density of incident laser beam. According to this relationship, a slope n of the log(I_{UC}) and log(P) can be determined as shown in Figure 4.7.

As follow from the calculated slopes - n of lines determined from the experimental data, the observed upconversion in prepared samples is at least two-photon process for both samples KYM:1%Er^{3+}/30%Yb^{3+} and KYM:1%Er^{3+}/50%Yb^{3+}. In Figure 4.7, the values of slopes equal to, or above 2, for the green band related to $^2H_{11/2}\rightarrow{}^4I_{15/2}$ (532nm) and $^2S_{3/2}\rightarrow{}^4I_{15/2}$ (546nm) transition, indicate that three-photon process is responsible for the excitation to the $^2H_{11/2}$ state and the $^2S_{3/2}$ state. While the red emission at around 653 nm corresponding to the $^4F_{9/2}\rightarrow{}^4I_{15/2}$ transition, it is a two-photon process.

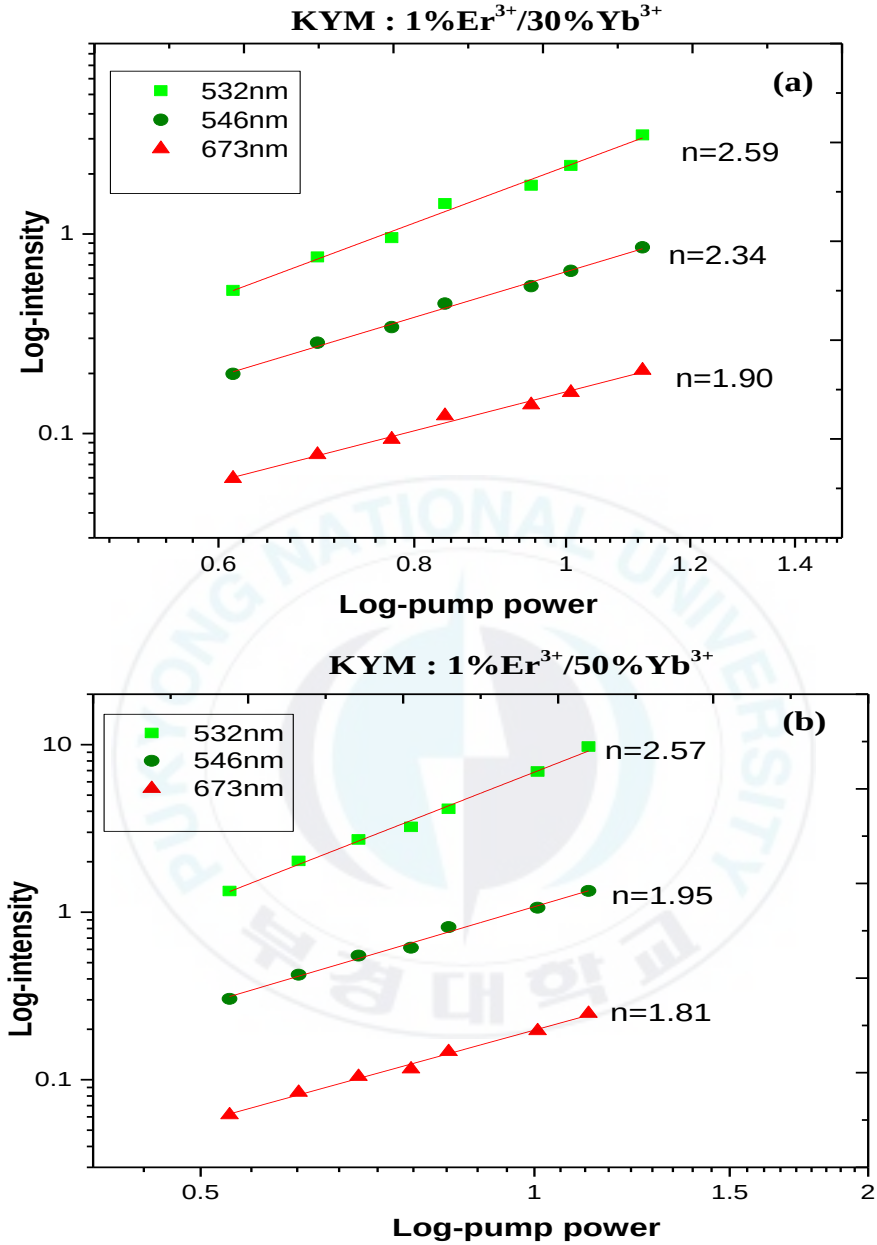

Figure 4.7 Power dependencies of integral luminescence intensities: (a) KYM : 1%Er^{3+}/30%Yb^{3+} and (b) KYM : 1%Er^{3+}/50%Yb^{3+}.

It should be noted that the n values for the sample KYM:1%Er^{3+}/30%Yb^{3+} is higher than that in the samples KYM:1%Er^{3+}/50%Yb^{3+}.

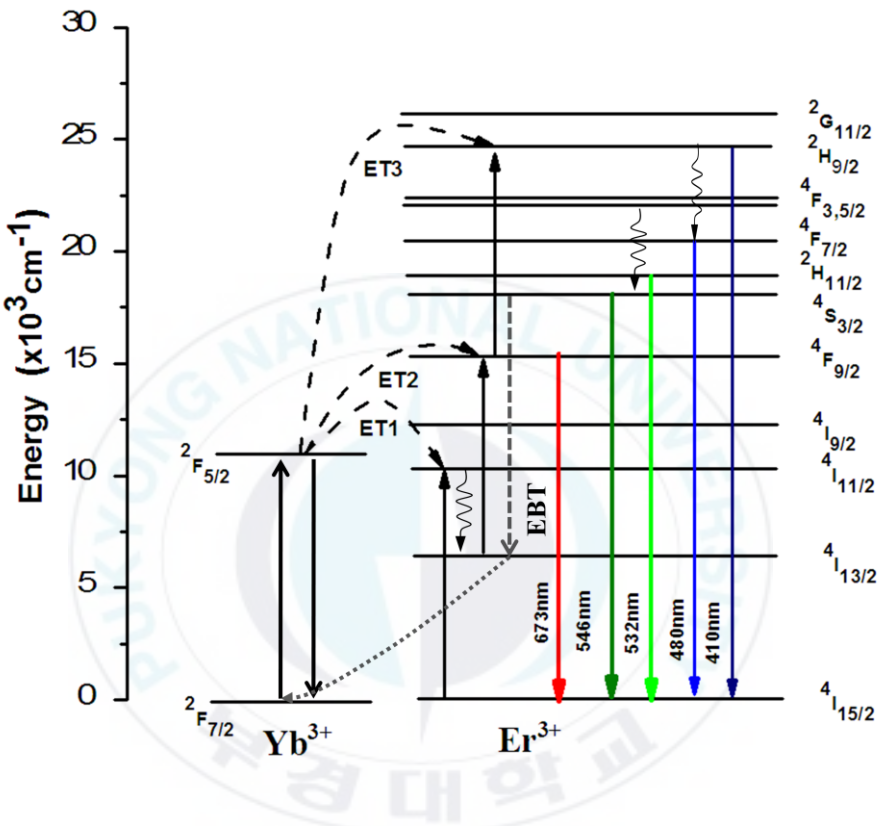

Figure 4.8 Energy level diagram illustrating the proposed energy migration mechanisms of Er^{3+}/Yb^{3+}

The mechanism of upconversion in $KY(MoO_4)_2$: Er^{3+}/Yb^{3+} samples is schematically presented in Fig. 4.8. The excitation at 975 nm results in the emission of Er^{3+}, for which the energy transfers upconversion mechanism is responsible. Yb^{3+} ions act as sensitizers to NIR radiation and donors to the Er^{3+} luminescence activators and simultaneously acceptors of absorbed

energy.

For the series $KY(MoO_4)_2$:1%Er^{3+}/x%Yb^{3+}, it can be seen that the blue and red emission are weaker than the green emissions, and the UC emission intensity increases with increasing working current of the 975 nm laser. The main possible upconversion mechanisms for Er^{3+}/Yb^{3+} codoped in $KY(MoO_4)_2$ is energy transfer (ET). From Figure 4.8, an Er^{3+} ion is excited initially from the ground state $^4I_{15/2}$ to the excited state $^4I_{11/2}$ through ESA (when Yb^{3+} concentration is small) or energy transfer (ET1) from Yb^{3+} to Er^{3+} (when Yb^{3+} concentration is high). From Fig 4.8, it is noted that the population of Er^{3+} at $^4I_{13/2}$ is related to the green and red emission, so we consider two kinds of the process may occur for the locating of Er^{3+} at $^4I_{13/2}$. Firstly, it's from nonradiative from the short lifetime level Er^{3+} locating at $^4I_{11/2}$ through ESA process or energy transfer (ET1) from Yb^{3+}. Secondly, the population of Er^{3+} at $^4I_{13/2}$ is from the energy back transfer (EBT) of Er^{3+} from $^4S_{3/2}$ level. In this case, because of the large energy gap between the $^4I_{11/2}$ and $^4I_{13/2}$ level of Er^{3+}, so the nonradiative process is possible but very small. So the EBT is the dominant process which occurs for the population of Er^{3+} at $^4I_{13/2}$.

For blue emission centered at 410 nm, the excitation processes involving the state at $^4I_{13/2}$ (Er^{3+}) are excited state by energy transfer ET2 and ET3 where excited Yb^{3+} ions ($^4F_{5/2}$ level) transfer this energy to Er^{3+} ions, promoting their excited electrons to $^2H_{9/2}$. Then, the excited electrons in the $^2H_{9/2}$ level give a relaxation to the ground state followed by the emission at 410 nm. For the emission band centered at 480 nm, after

being excited to $^2H_{9/2}$, the electrons may give a fast nonradiative to a lower level at $^2H_{7/2}$ then relax to ground state at followed by emitting a 480 nm photons.

For green emission, the excited electrons at the $^2H_{9/2}$ level give a fast nonradiative relaxation to the $^2H_{11/2}$ and the $^4S_{3/2}$ state followed by relaxing to the ground state and emitting green photons: 532 nm corresponding $^2H_{11/2} \rightarrow {}^4I_{15/2}$ transition, 546 nm corresponding $^4S_{3/2} \rightarrow {}^4I_{15/2}$ transition.

For the red emission originating in the energy level $^4F_{9/2}$, after ET1, ET2 process, the Er^{3+} ions relax from $^4F_{9/2}$ to ground state and emit a 673 nm photons.

Because of the blue emission centered at 410 and 480 nm which are too weak, they are ignored. We focus on the green and red emission band corresponding to the transition $^2H_{11/2}$ / $^4S_{3/2} \rightarrow {}^4I_{15/2}$ and $^2F_{9/2} \rightarrow {}^4I_{15/2}$. From Figure 4.7, the logarithmic plot of the integrated emission intensities of the upconversion band in the region of visible light, i.e. red and green emission intensities as a function of the incident power density. The output slopes (n) for green band centered at 532 and 546 nm of the sample $KY(MoO_4)_2$: $1\%Er^{3+}/30\%Yb^{3+}$ are 2.59 and 2.34, respectively, while the slope values of the sample $KY(MoO_4)_2$: $1\%Er^{3+}/50\%Yb^{3+}$ are 2.57 and 1.95 for emission band centered at the same wavelength. It indicated that three and two photons processes are responsible for the populating of $^2H_{11/2}$ and $^4S_{3/2}$, as shown in the energy level diagram in Figure 4.8. While, for red emission the output slopes (n) of the sample $KY(MoO_4)_2$: $1\%Er^{3+}/30\%Yb^{3+}$ and $KY(MoO_4)_2$: $1\%Er^{3+}/50\%Yb^{3+}$ are 1.90 and 1.81, respectively. It indicates

that two photons process is responsible for emitting 673 nm photons.

It is interesting to find that for both sample $KY(MoO_4)_2$: 1%Er^{3+}/x%Yb^{3+}, the slope values decrease when the Yb^{3+} concentration increase. To better understanding the reason of the decreasing of slope value, we have to consider the population of Er^{3+} in every excited state. These can be explained based on the [27, 28] anomalous behavior which is induced by the competition between population and depopulation process for the depletion of the intermediate excited states when high Yb^{3+} concentration and high power density. Figure 4.9 shows the dependence of slope value (n) on the Yb^{3+} concentration.

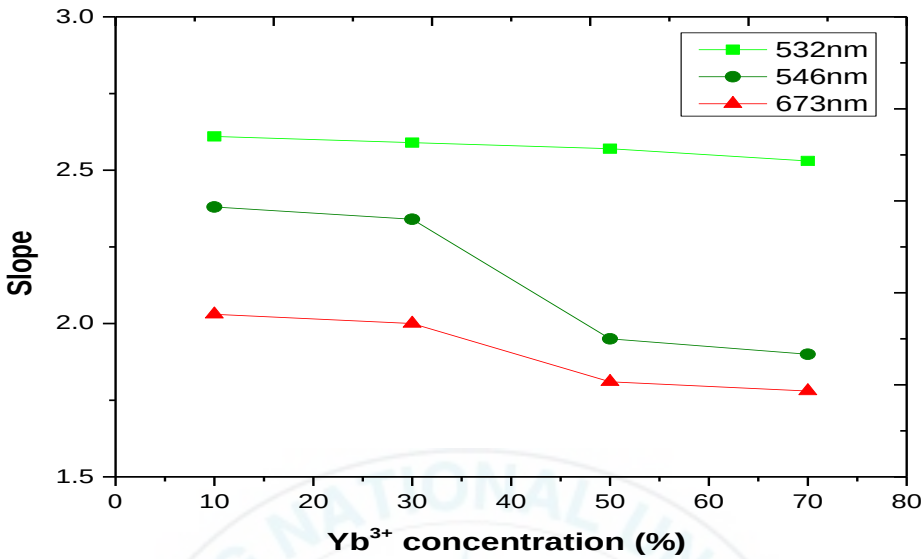

Figure 4.9 Dependence of slope value (n) on the Yb^{3+} concentration

To better understand the influence of pump power and Yb^{3+} concentration on the luminescence intensity, a discussion was informed by Suyver in 2005 [27, 28] to investigate the anomalous power dependence of sensitized upconversion luminescence.

A simplified model of upconversion energy transfer process between the sensitizer and the activator was given in Figure 4.10 to describe the phenomenon happening in an energy transfer process.

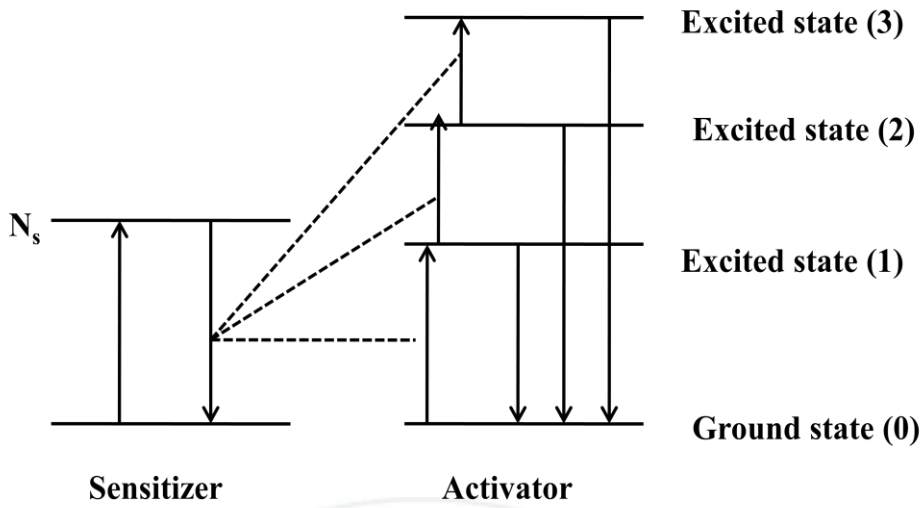

Figure 4.10 Schematic presentation of the energy transfer processes that can occur in the simplified model.

Under 975 nm excitation of the laser with the incident pump power P. When P donates the laser power and σ the excitation cross section for the sensitizer ions, the steady population of excited sensitizer ions, N_s, is given by

$$N_s=\sigma P \quad (1)$$

Then the sensitizer transfers its energy to the activator through energy transfer process (ET). The activator is excited to jump to the excited state (i). Let N_i be the steady population of excited sensitizer ion at the excited state (i), W_i is the upconversion rate constant associated with up-conversion from the state (i) to (i+1) of activator and R_i is relaxation rate constant of activator from the state (i) to ground state. As a result of energy transfer we have:

$$N_1 \sim N_s \quad (2)$$

From that hypothesis, we obtained the balance equation for the steady state population density of state (i) of the activator ion:

$$W_{i-1}N_{i-1}N_s = (R_i + W_iN_s)N_i \quad (3)$$

From equation (3), we get N_i be the steady population of excited sensitizer ion at the excited state (i):

$$N_i = \frac{W_{i-1}N_{i-1}N_s}{R_i + W_iN_s} \quad (4)$$

At low power and low Yb^{3+} doping concentration

At low power and low Yb^{3+} doping concentration, low energy is transferred from Yb^{3+} to Er^{3+} then upconversion from the state (i) to state (i+1) can be ignored as the relaxation to the ground state will be the dominant depopulation process, so $R_i >> W_iN_s$. The equation (4) becomes

$$N_i = \frac{W_{i-1}N_{i-1}N_s}{R_i} \quad (5)$$

We totally can obtain the similar equation for the steady population of excited sensitizer ion at the excited (i-1) N_{i-1}:

$$N_{i-1} = \frac{W_{i-2}N_{i-2}N_s}{R_{i-1}} \quad (6)$$

From equation (5) and (6) we get:

$$N_i = \frac{W_{i-1}N_s}{R_i}\frac{W_{i-2}N_{i-2}N_s}{R_{i-2}} = \frac{W_{i-1}W_{i-2}N_{i-2}}{R_iR_{i-1}}N_s^2 \quad (7)$$

From equation (7), we can obtain that the N_i depends nonlinearly on the N_s, the final result becomes

$$N_i \sim (N_s)^i \sim P^i \quad (8)$$

At high power and high Yb^{3+} doping concentration

At high pump power and high Yb^{3+} concentration, the upconversion process from the state (i) to (i+1) is much more dominant because of more energy is transferred from Yb^{3+} to Er^{3+}. That leads to $W_iN_iN_s >> R_iN_i$. Equation (3) becomes

$$W_{i-1}N_{i-1}N_s = W_iN_iN_s \quad (9)$$

We obtain

$$N_i = \frac{W_{i-1}}{R_i} N_{i-1} \sim N_{i-1} \quad (10)$$

Note that $N_i \sim N_{i-1}$, combine with equation (1) and (2) this equivalence can be written:

$$N_i \sim N_s \sim P^1 \quad (11)$$

where P remains the laser power.

From equation (8) and equation (11), we can conclude that when pump power and the sensitizer concentration (Yb^{3+} concentration) increase, the slope value decrease from the n value to 1 due to the competitive of the upconversion processes and the relaxation processes. That is the explanation for the decrease of n when the Yb^{3+} increases in Figure 4.9.

5. Summary and Conclusions

In conclusion, the compound samples $KY(MoO_4)_2$: $1\%Er^{3+}$/ $x\%Yb^{3+}$ ($5 \leq x \leq 99$) were synthesized successfully by solid state reaction method. The structure of the solid solution series was carried out by X-ray powder diffraction. Under a 975 nm excitation, the upconversion luminescence shows a strong green band which agrees with the transition $^2H_{11/2}$/ $^4S_{3/2} \rightarrow {}^4I_{15/2}$ of Er^{3+} and a weak red band which corresponds to the transition $^2F_{9/2} \rightarrow {}^4I_{15/2}$ of Er^{3+}. The ETU is the main route of the upconversion processes and the reduced green and red upconversion photoluminescence of the sample at 50% mol% of Yb^{3+} is due to the concentration quenching of Yb^{3+}. Two excitation processes are responsible for red emission and three excitation processes are responsible for green emission. When the Yb^{3+} concentration increases, the slope value decreases due to the competitive of the upconversion processes and the relaxation processes.

6. References

[1] J. Méndez-Ramos, V. K. Tikhomirova, V. D. Rodrígueza, and D. Furnissb, Alloys Compounds. **440,** 328. (2007).

[2] F. Heine, E. Heumann, T. Danger, T. Schweizer, J. Koetke, G. Huber, and B. H. T. Chai, Solid State Lasers OSA Proc. Series. **55** (1994).

[3] M. Frenz, Ch. Mischler, V. Romano, M. Forrer, O. M. Müller, and H. P. Weber, Phys. B. **52,** 251 (1991).

[4] Y. Kishi, S. Tanabe, S. Tochino, and G. Pezzotti, J. Am. Ceram. Soc. **88,** 3423 (2005).

[5] J. H. Zhang, H.Z. Tao, Y. Chang, and X.J. Zhao, J. Rare Earth. **25**, 108 (2007).

[6] X. Li, Q. Li, J. Wang, and J. Li, J. Lumin. **124,** 351 (2007).

[7] L. Zhang, H. Hu, C. Qi, and F. Lin, Opt. Mater. **17,** 371 (2001).

[8] S. Shionoya, W. M. Yen, and H. Yamamoto, Phosphor handbook. CRC press (2006).

[9] J. G. Solé, L.E. Bausá, and D. Jaque, An introduction to the optical spectroscopy of inorganic solids. John Wiley & Sons (2005).

[10] G. Liu, and B. Jacquier, Spectroscopic properties of rare earth in optical materials. **83**. Springer Science & Business Media (2006).

[11] G. Blasse, and B. C. Grabmaier, Luminescent materials. Springer Science & Business Media, (2012).

[12] Y. K. Voron'ko, E. V. Zharikov ; D. A. Lis, A. A. Sobol, K. A. Subbotin, S. N. Ushakov, V. E. Shukshin, Laser Optics 2003: Solid State Lasers and Nonlinear Frequency Conversion. International Society for Optics and Photonics (2004).

[13] C. Cascales, A. Méndez Blas, M. Rico, V. Volkov, and C. Zaldo, Optical Materials. **27,** 1672-1680 (2005).

[14] J. P. M. Van Vliet , G. Blasse, L. H. Brixner, J. Solid State Chem. **76,** 160-166 (1998).

[15] H. Yamamoto, S. Seki, and T. Ishiba, J. Solid state Chem. **94**, 396 (1991)

[16] T. Förster; Ann. Phys. **2**, 55 (1948).

[17] D. L. Dexter, J. Chem.. Phys. **21**,836 (1953).

[18] M. Inokuti and F. Hirayama, J. Chem. Phys.**43**, 1978 (1965)

[19] T. P. J. Botden, and Philips res. Rep. **7**, 197 (1952).

[20] D. L. Dexter and J. H. Schulman, J. Chem. Phys. **22**, 1063 (1954).

[21] F. Auzel, Chem. Rev. **104**, 139 (2004).

[22] Y. Mita, “Phosphor Handbook”, CRC Press (2007).

[23] D. R. Gamelin, and H. U. Gudel, Transition metal and rare earth compound, Springer Berlin Heidelberg. **214,** 1-56 (2001).

[24] L. Zhang, H. Hu, C. Qi, and F. Lin, Optical Materials. **17**, 371-377 (2001)

[25] Y. Wang, L. Tu, J. Zhao, Y. Sun, X. Kong, and H. Zhang, J. Phys. Chem. C. **113,** 7164-7169 (2009).

[26] G. F. Knoll, Radiation Detection and Measurement, Wiley, New York, (1979).

[27] M. Pollnau, D. R. Gamelin, S. R. Lüthi, H. U. Güdel, and M. P. Hehlen, Phys. Rev. B. **61**, 3337 (2000).

[28] J. F. Suyver, A. Aebischer, S. García-Revilla, P. Gerner, and H. U. Güdel, Phys. Rev. B. **71**, 123-125 (2005).

[29] R. D. Shannon, Acta Cryst. **A32**, 751-767 (1976).

Acknowledgment

The work presented in this thesis was performed in the Laboratory of Luminescence Materials, belong to Interdisciplinary Program of Biomedical Engineering, Pukyong National University.

First and foremost, I would like to express my gratitude to my supervisor, Prof. Hyo Jin Seo, a respectable, responsible and resourceful scholar, who helped me to finish this study, gave me more useful and valuable academic guidance and advice. Prof. Seo spent much time on communicating and discussing with me about the experiment and the results. It's so meaningful to me to complete my thesis. Without his help, this thesis would not have been completed.

I would like to express my deep thanks to all of my labmates: Dr. Xiangfu Wang, Peiqing Cai, Lin Qin, Culi Chen, Han Cheng, Jing Wang and Hang Thi Dang, who always try their best to help me work out many problems in the study and living life in Korea. I have a wonderful life in Busan because of them.

Finally, I would like to dedicate this work to my family, who always encouraged me during the whole course of my study. Although they are in

Vietnam, they care about my living, my study by their heart. I'm so appreciated about that.